Rapid Communications | Editors' Suggestion

An anomalous higher-order topological insulator

S. Franca,[1] J. van den Brink,[1,2] and I. C. Fulga[1]
[1]*Institute for Theoretical Solid State Physics, IFW Dresden, 01171 Dresden, Germany*
[2]*Institute for Theoretical Physics, TU Dresden, 01069 Dresden, Germany*

(Received 26 July 2018; published 28 November 2018)

Topological multipole insulators are a class of higher-order topological insulators (HOTIs) in which robust fractional corner charges appear due to a quantized electric multipole moment of the bulk. This bulk-corner correspondence has been expressed in terms of a topological invariant computed using the eigenstates of the Wilson loop operator, a so-called "nested Wilson loop" procedure. We show that, similar to the unitary Floquet operator describing periodically driven systems, the unitary Wilson loop operator can realize "anomalous" phases that are topologically nontrivial despite having a trivial topological invariant. We introduce a concrete example of an anomalous HOTI, which has a quantized bulk quadrupole moment and fractional corner charges, but a vanishing nested Wilson loop index. An invariant able to capture the topology of this phase is then constructed. Our work shows that anomalous topological phases, previously thought to be unique to periodically driven systems, can occur and be used to understand purely time-independent HOTIs.

DOI: 10.1103/PhysRevB.98.201114

Introduction. In topological insulators, bulk-boundary correspondence relates the presence of robust boundary phenomena to a quantity determined from the bulk system, a topological invariant [1–5]. In strong topological insulators, the D-dimensional bulk is gapped and the topological invariant counts the number of gapless modes present on the $(D-1)$-dimensional boundaries of the crystal. In the recently introduced higher-order topological insulators (HOTIs) [6–31], however, both the bulk and the boundaries are gapped, so that standard bulk-boundary correspondence no longer applies. In some cases, the HOTI invariant determines the presence of topologically protected gapless modes on some regions of the boundary which have dimensions $(D-2)$ or less, such as the corners or hinges of a crystal [9–19,32].

Gapless modes on corners or hinges are not the only manifestations of topology in a HOTI, however. Extending the notion of bulk-boundary correspondence to that of bulk-hinge or bulk-corner correspondence allows for a greater variety of boundary phenomena to be associated with a topologically nontrivial bulk. In seminal works, Benalcazar *et al.* have introduced a class of HOTIs dubbed "quantized electric multipole insulators" [6,7], whose nontrivial nature leads to topologically protected corner *charges*, not states. Among others, they considered a two-dimensional (2D) topological quadrupole insulator (TQI), whose topological invariant is a bulk quadrupole moment q_{xy}. The latter is quantized to 0 (trivial) or $\frac{e}{2}$ (nontrivial) by lattice symmetries, with e the electron charge. This leads to quantized tangential edge polarizations and fractional corner charges. The defining relation of this HOTI is

$$q_{xy} = \left|p_x^{\text{edge}}\right| = \left|p_y^{\text{edge}}\right| = |Q_{\text{corner}}|, \tag{1}$$

where p_x^{edge} and p_y^{edge} are the tangential polarizations per unit length of the x and y edge and Q_{corner} is the fractional corner charge. The above relations illustrate the bulk nature of the TQI, distinguishing it from phases in which the corner charge arises only due to "free" electric dipoles at the boundaries [6]. In the latter case, $Q_{\text{corner}} = p_x^{\text{edge}} + p_y^{\text{edge}}$, violating Eq. (1).

To compute the bulk quadrupole moment, Refs. [6,7] use the Wilson loop, a unitary operator whose spectrum represents the Wannier centers of electronic wave functions in the crystal. In the TQI these centers form gapped Wannier bands, and the quadrupole moment is determined from a topological invariant associated with these bands. An essential observation in the context of this Rapid Communication is that this procedure, termed a "nested Wilson loop" formalism, is unlike those used for conventional topological phases. It determines the invariant from the eigenstates of a unitary operator and not directly from those of the Hermitian, Hamiltonian operator.

The topological phases of *unitary* operators are well studied in the context of periodically driven systems [33–44], which are usually described in terms of the time evolution operator over one driving period—the Floquet operator. Its unitary nature means the spectrum is 2π periodic, enabling so-called "anomalous topological phases" [33,39–44]. In the latter, the invariant associated with the Floquet operator vanishes, failing to capture the topologically nontrivial nature of the bulk. Anomalous topological phases so far have been hallmarks of periodically driven systems, and are considered impossible to achieve in a time-independent setting. Ultimately, however, their presence is possible solely due to the fact that nontrivial topology is realized using a unitary operator instead of a Hermitian one. Is it then possible for the unitary Wilson loop of a HOTI to host such anomalous phases?

In this Rapid Communication, we show that time-independent HOTIs can indeed host anomalous phases, introducing a class of systems we dub *anomalous HOTIs*. Using the familiar language of Majorana bound states, we build a model of an electric insulator with a quantized bulk quadrupole moment and fractional corner charges. The system obeys the TQI relation Eq. (1), but has a vanishing nested Wilson loop

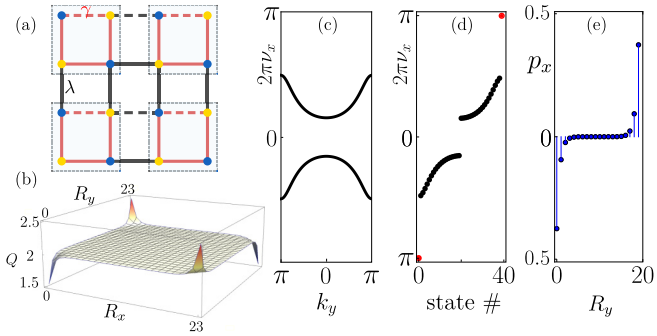

FIG. 1. (a) TQI described by Eq. (2). Solid/dashed lines represent hoppings with positive/negative amplitudes, the red lines represent intracell hoppings γ, and the black ones intercell hoppings λ. Unit cells are marked by gray squares, with blue and yellow circles denoting sites belonging to different sublattices. (b) Charge density (Q) plot for a finite system consisting of 24×24 unit cells, where R_x and R_y label the unit cells in real space. The excess corner charge is $\pm 1/2$. (c) Bulk Wannier bands of $\mathcal{W}_{x,\mathbf{k}=(\pi,\pi)}$, obtained by discretizing the BZ using 51 k points. (d) Wannier spectrum in the strip geometry (infinite in x, 20 unit cells in y). The $\nu = \pm 0.5$ edge modes are shown in red. (e) Tangential polarization along x as a function of position in the y direction, R_y. The integrated polarization over half of the lattice sites yields $\pm 1/2$. We use $\gamma = 0.5$ and $\lambda = 1$. As explained in Refs. [6,7], to fix a sign for the polarization and the corner charges, we add a term $\delta\tau_z\sigma_0$ to Eq. (2) ($\delta = 10^{-3}$), which weakly breaks the two mirror symmetries $\mathcal{M}_x$ and $\mathcal{M}_y$ but not their product, the inversion symmetry $\mathcal{I} = \mathcal{M}_x\mathcal{M}_y$.

invariant. We then adapt this formalism and formulate an invariant which correctly captures the topologically nontrivial nature of the phase.

Nested Wilson loops. We begin by briefly reviewing the previously introduced TQI and the nested Wilson loop procedure [6,7]. We consider a system of spinless, noninteracting fermions on a square lattice with dimerized nearest-neighbor hoppings and a π flux threading every plaquette [see Fig. 1(a)]. Setting $\hbar = 1$ and the lattice constant $a = 1$, the Hamiltonian is

$$h(\mathbf{k}) = (\gamma + \lambda\cos k_x)\tau_x\sigma_0 - \lambda\sin k_x\tau_y\sigma_z - (\gamma + \lambda\cos k_y)\tau_y\sigma_y - \lambda\sin k_y\tau_y\sigma_x, \quad (2)$$

where $\mathbf{k} = (k_x, k_y)$, τ Pauli matrices act on the sublattice degree of freedom, and σ's parametrize the degree of freedom associated with the two sites within a sublattice. Intracell and intercell hoppings are γ and λ, respectively.

For $|\gamma| < |\lambda|$, the system obeys all the requirements of a TQI, Eq. (1). The 2D bulk is gapped and each edge forms a nontrivial Su-Schrieffer-Heeger (SSH) chain [45], leading to a single protected zero mode at every corner. At half filling, there are $N_{\text{occ}} = 2$ occupied bands in the bulk and the four degenerate corner states contain two electrons in total, leading to a fractional corner charge $|Q_{\text{corner}}| = 1/2$ [see Fig. 1(b)], where we set the electron charge $e = 1$ throughout the following.

To determine the polarizations, we define Wilson loop operators describing parallel transport of eigenstates along a closed path p in the Brillouin zone (BZ). In the thermodynamic limit, the Wilson loop [46,47] is a path-ordered exponential (denoted $\overline{\exp}$)

$$\mathcal{W}_p = \overline{\exp}\left(-i\oint_p dp\cdot\mathcal{A}_{\mathbf{k}}\right), \quad (3)$$

where $\mathcal{A}_{\mathbf{k}}$ is the Berry connection of the occupied Hamiltonian eigenstates $|u_{\mathbf{k}}\rangle$. As such, $\mathcal{A}_{\mathbf{k}}$ is an $N_{\text{occ}} \times N_{\text{occ}}$ matrix with elements $[\mathcal{A}_{\mathbf{k}}]^{mn} = -i\langle u^m_{\mathbf{k}}|\nabla_{\mathbf{k}}u^n_{\mathbf{k}}\rangle$. We only consider Wilson loops computed on noncontractible paths of the BZ (so-called large Wilson loops). We define $\mathcal{W}_{x,\mathbf{k}}$ on a path along k_x, from $\mathbf{k}$ to $\mathbf{k} + (2\pi, 0)$, and similarly $\mathcal{W}_{y,\mathbf{k}}$ from $\mathbf{k}$ to $\mathbf{k} + (0, 2\pi)$, where $\mathbf{k}$ is called the base point of the Wilson loop. Diagonalizing these unitary operators,

$$\mathcal{W}_{x,\mathbf{k}}\left|\nu^j_{x,\mathbf{k}}\right\rangle = \exp\left[i2\pi\nu^j_x(k_y)\right]\left|\nu^j_{x,\mathbf{k}}\right\rangle, \quad (4)$$

where $j \in \{1, \ldots, N_{\text{occ}}\}$, yields eigenstates $|\nu^j_{x,\mathbf{k}}\rangle$ with components $[\nu^j_{x,\mathbf{k}}]^n$ as well as eigenphases ν^j_x. Note that while in general eigenstates depend explicitly on the base point $\mathbf{k}$, the eigenvalues are independent of the momentum along the path. As such, ν^j_x is only a function of k_y, while the eigenphase of $\mathcal{W}_{y,\mathbf{k}}$, ν^j_y, only depends on k_x. Since the model Eq. (2) has a fourfold rotation symmetry, we will only focus on $\mathcal{W}_{x,\mathbf{k}}$ in the remainder of this section, with the understanding that $\mathcal{W}_{y,\mathbf{k}}$ gives identical results.

We numerically determine the Wilson loop operators by discretizing the BZ. The procedure is thoroughly explained in Refs. [6,7], so we do not repeat it here. In the Supplemental Material [48], however, we give a detailed account of these steps and include the code library we have developed for this purpose, which is general enough to be used for a large variety of HOTIs. The two eigenphases ν^j_x obtained from Eq. (4) are shown in Fig. 1(c). They form gapped Wannier bands which are positioned symmetrically around 0, which is a consequence of the two mirror symmetries $\mathcal{M}_x = \tau_x\sigma_z$ and $\mathcal{M}_y = \tau_x\sigma_x$ acting in the x and y directions, respectively. Since the bulk polarization is given by the sum of Wilson loop eigenphases, $p_x(k_y) = \sum_j \nu^j_x(k_y)$, it vanishes at every momentum, a necessary requirement for a TQI [6,7]. Of course, due to fourfold rotation the same result holds for $p_y(k_x)$.

The key insight behind the nested Wilson loop formalism is to notice that, since the Wannier bands are gapped, they carry their own topological invariants. Nontrivial Wannier bands then lead to topologically protected Wannier modes at the boundaries of the system. To introduce boundaries, we consider Eq. (2) in a strip geometry, infinite along k_x and containing 20 unit cells in the y direction. From the strip Hamiltonian $h(k_x, R_y)$, where R_y labels the unit cells, we compute the large Wilson loop along the only remaining momentum k_x and show its eigenphases in Fig. 1(d). The gapped Wannier centers are accompanied by topological modes (shown in red) which are pinned to $\nu_x = \pm 0.5$ by mirror symmetry. These are localized on opposite boundaries of the system, leading to a quantized edge polarization. We confirm this in Fig. 1(e), which shows the tangential polarization p_x in the strip geometry. While there is no polarization in the bulk, the boundaries have a quantized polarization $\pm 1/2$, which accompanies the fractional corner charges.

Since $|p_x^{\text{edge}}| = |p_y^{\text{edge}}| = |Q_{\text{corner}}| = 1/2$, the origin of the corner charges must be due to a bulk quadrupole moment $q_{xy} = 1/2$. To compute the latter, Refs. [6,7] use the topological invariants associated with the Wannier bands in Fig. 1(c). They split the Wannier bands into two sectors, an "occupied" and an "unoccupied" one,

$$\begin{aligned} \nu_x^- &= \left\{\nu_x^j(k_y) \ \text{ such that } \ \nu_x^j(k_y) < 0\right\}, \\ \nu_x^+ &= \left\{\nu_x^j(k_y) \ \text{ such that } \ \nu_x^j(k_y) > 0\right\}. \end{aligned} \tag{5}$$

Notice that, similar to Floquet systems, this distinction is not well defined, since the whole spectrum is 2π periodic, and there is no notion of a band being "above" or "below" another. Nevertheless, this splitting allows one to separate the space of occupied Hamiltonian eigenstates into two Wannier band subspaces, corresponding to Wannier states

$$\left|w_{x,\mathbf{k}}^{\pm,r}\right\rangle = \sum_{n=1}^{N_{\text{occ}}} \left|u_{\mathbf{k}}^n\right\rangle \left[v_{x,\mathbf{k}}^{\pm,r}\right]^n. \tag{6}$$

Here, the superscript $\pm$ denotes the Wannier band subspace, with $r \in \{1, \ldots, N_{\text{occ}}/2\}$ labeling the bands within a subspace. The nontrivial nature of each of the Wannier subspaces is then determined from the Wannier sector polarization. In the thermodynamic limit,

$$p_y^{\nu_x^\pm} = -\frac{1}{(2\pi)^2} \int_{\text{BZ}} \text{Tr}\left[\tilde{\mathcal{A}}_{y,\mathbf{k}}^{\nu_x^\pm}\right] d^2\mathbf{k} \tag{7}$$

is a $\mathbb{Z}_2$ topological index, $p_y^{\nu_x^\pm} \in \{0, 1/2\}$, where $\left[\tilde{\mathcal{A}}_{y,\mathbf{k}}^{\nu_x^\pm}\right]^{mn} = -i \left\langle w_{x,\mathbf{k}}^{\pm,m}\right| \partial_{k_y} \left|w_{x,\mathbf{k}}^{\pm,n}\right\rangle$ are the matrix elements of the $(N_{\text{occ}}/2) \times (N_{\text{occ}}/2)$ Berry connection of the $\pm$ Wannier subspace. In the case of Eq. (2), $N_{\text{occ}} = 2$ so the connection is a scalar. We find $p_y^{\nu_x^\pm} = p_x^{\nu_y^\pm} = 1/2$, in agreement with Refs. [6,7], which define the bulk quadrupole invariant as

$$q_{xy} = p_y^{\nu_x^+} p_x^{\nu_y^+} + p_y^{\nu_x^-} p_x^{\nu_y^-}, \tag{8}$$

obtaining a quantized value $q_{xy} = 1/2$.

Anomalous HOTI. In a HOTI, nontrivial Wannier sector invariants, Eq. (7), imply topological Wannier edge modes, leading to quantized edge polarizations and fractional corner charges. The converse statement is, however, not true. As we show in the following, due to the unitary nature of the Wilson loop, Wannier edge modes can occur even if the subspaces $\nu_x^\pm$ have trivial invariants.

To model an anomalous HOTI, we consider a 2D array of Majorana nanowires [49,50]. The wires are coupled to each other in a dimerized fashion, such that their end modes gap out in pairs, leaving topologically protected zero modes only at the corners [see Fig. 2(a)]. In this respect, the system is very similar to the TQI of Eq. (2): Each corner state is a simultaneous topological mode of two nontrivial edges. The horizontal edges of Fig. 2(a) are topological nanowires, while the vertical edges are Kitaev chains in the nontrivial phase [51]. The Hamiltonian reads

$$\begin{aligned} H(\mathbf{k}) = {} & [2t_x(1 - \cos k_x) - \mu]\tau_z\sigma_0\eta_0 \\ & + V_z\tau_0\sigma_z\eta_0 + \Delta\tau_x\sigma_0\eta_0 + \alpha \sin k_x \tau_z\sigma_y\eta_0 \\ & - \beta_1\tau_z\sigma_x\eta_y - \beta_2 \sin k_y \tau_z\sigma_x\eta_x + \beta_2 \cos k_y \tau_z\sigma_x\eta_y, \end{aligned} \tag{9}$$

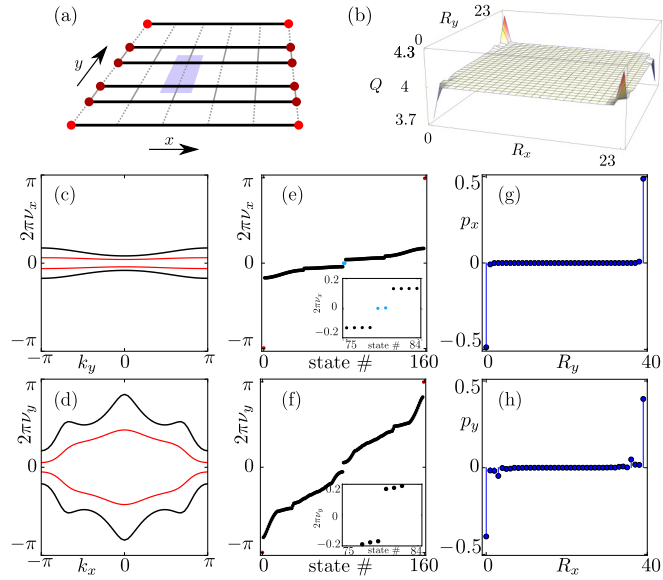

FIG. 2. (a) Array of Majorana wires (black lines), coupled in a dimerized fashion (gray solid/dashed lines). The unit cell (blue) contains two wires. Majorana modes which are gapped out by the dimerized coupling are shown in dark red, whereas protected corner modes are shown in bright red. (b) Charge density plot of a system of 24×24 unit cells. The integrated excess charge is $\pm 1/2$ for each corner. (c), (d) Bulk Wannier bands of $\mathcal{W}_{x,(\pi,\pi)}$ and $\mathcal{W}_{y,(\pi,\pi)}$. (e), (f) Wannier spectra in a strip geometry, infinite along either (e) k_x or (f) k_y, with 40 unit cells in the finite direction. Both spectra show edge modes at $\nu = \pm 0.5$ (red), but the strip along k_x also shows topological 0 modes (blue). The insets show closeups of the gaps around $\nu = 0$. (g), (h) The corresponding edge polarization is quantized to $\pm 1/2$ in both cases. To fix the sign of the charge and polarization, we add a mirror symmetry breaking term $\delta\tau_y\sigma_y\eta_z$ ($\delta = 10^{-2}$).

where t_x and α are the nearest-neighbor hopping strength and the spin-orbit coupling (SOC) strength in the x direction (along the wires), μ is the chemical potential, V_z is the Zeeman energy, and Δ is the superconducting pairing strength. In the y direction, $\beta_1 < \beta_2$ are dimerized Rashba SOC terms connecting neighboring wires within and between unit cells, whereas Pauli matrices τ, σ, and η act on the particle-hole, spin, and wire space, respectively. We set $\alpha = 3.7$, $t_x = 1.7$, $\mu = -0.9$, $\Delta = 1.6$, $V_z = 2.7$, $\beta_1 = 0.8$, and $\beta_2 = 6.2$ throughout the following.

As is conventional when describing the topology of superconductors [52,53], in the following we neglect the Bogoliubov–de Gennes (BdG) nature of the Hamiltonian Eq. (9), treating it instead as a charge-conserving Bloch Hamiltonian with a well-defined filling. As such, from now on we consider each of the four corner modes *not* as a Majorana bound state, but as an electron state which may be filled independently of the others. At half filling, there are $N_{\text{occ}} = 4$ occupied bulk bands, and each corner mode is half filled, such that $|Q_{\text{corner}}| = 1/2$ [see Fig. 2(b)], the first indication of a TQI.

We follow the procedure summarized in the previous section, and determine the bulk and edge polarizations. Since Eq. (9) lacks rotation symmetry, we show the eigenphases

of both $\mathcal{W}_{x,(\pi,\pi)}$ and $\mathcal{W}_{y,(\pi,\pi)}$ in Figs. 2(c) and 2(d). There are four Wannier bands in total, such that each Wannier sector [Eq. (5)] contains two bands, shown in red and black. Similarly to the TQI of Eq. (2), the bands are gapped and positioned symmetrically around 0 due to mirror symmetries (here, $\mathcal{M}_x = \eta_z\sigma_z$ and $\mathcal{M}_y = \eta_y$), which leads to a vanishing bulk polarization. The behavior of $\mathcal{W}_{y,(\pi,\pi)}$ is identical to that of the previous model: Topological Wannier edge modes appear at $\nu_y = \pm 0.5$ [Fig. 2(f)], leading to edge polarizations which are quantized to $\pm 1/2$ [Fig. 2(h)].

The crucial difference with respect to Eq. (2) is given by the Wannier spectrum associated with $\mathcal{W}_x$ [Fig. 2(e)]. In a strip geometry infinite along k_x, the Wilson loop shows two *different* kinds of edge modes. The first (shown in red) corresponds to π eigenphases of the Wilson loop, $\nu = \pm 0.5$, leading to quantized edge polarizations. The second kind of topological edge mode (shown in blue) has $\nu = 0$ instead. Both 0 and π modes are compatible with the mirror symmetry, which renders the spectrum $\pm\nu$ symmetric. However, since the polarization is given by the eigenphases of the Wilson loop, the zero modes do not contribute to the edge polarizations, even though their eigenstates are localized on the boundaries of the system [48].

Figure 2(e) is analogous to the spectrum of a one-dimensional (1D) Floquet topological phase, where it is known that two kinds of protected modes can occur, at 0 and at π quasienergies, respectively [54–58]. When both types of topological boundary states are present in the same system, the resulting phase is termed "anomalous," since the topological invariant associated with the bulk Floquet operator vanishes. The same occurs for the Wilson loop operators of Fig. 2. For $\mathcal{W}_{y,(\pi,\pi)}$, only π modes are present so the Wannier sector polarizations [Eq. (7)] are $p_x^{\nu_y^\pm} = 1/2$, as expected. For $\mathcal{W}_{x,(\pi,\pi)}$, on the other hand, we find trivial Wannier subspace invariants $p_y^{\nu_x^\pm} = 0$.

Taken by themselves, the Wannier sector invariants would indicate a trivial HOTI, $q_{xy} = 0$, as per Eq. (8). We know, however, that this is not the case, since both of the bulk Wilson loops show topological edge modes when boundaries are introduced. These modes lead to quantized edge polarizations equal to the corner charge, $|p_x^{\text{edge}}| = |p_y^{\text{edge}}| = |Q_{\text{corner}}| = 1/2$, which is the defining relation of a TQI, Eq. (1). To overcome this discrepancy, we adapt the nested Wilson procedure and introduce a different bulk index. The key observation is that for the model Eq. (9) there are two Wannier bands in each of the $\nu_x^\pm$ subspaces, such that the associated Berry connection of each sector, $\tilde{\mathcal{A}}_{y,\mathbf{k}}^{\nu_x^\pm}$, is a 2×2 matrix. This means that the Wannier sector polarization Eq. (7) effectively sums the invariants of the two Wannier bands, so that two nontrivial bands lead to a vanishing topological index. We take this into account and compute the topological index of each band *separately*, splitting the trace in Eq. (7) into two separate integrals, $p_y^{\nu_x^\pm} = p_y^{\nu_x^\pm,1} + p_y^{\nu_x^\pm,2}$, where the superscript 1,2 denotes the index of the black and red Wannier bands of Figs. 2(c) and 2(d). Note that since the Wannier bands do not cross, the index of each band is well defined and quantized to 0 or 1/2 [48]. This allows us to redefine the bulk quadrupole index of Eq. (8) as

$$q_{xy} = \sum_{r=1}^{N_{\text{occ}}/2} p_y^{\nu_x^+,r}\, p_x^{\nu_y^+,r} + p_y^{\nu_x^-,r}\, p_x^{\nu_y^-,r}. \tag{10}$$

We find that in each Wannier sector both Wannier bands of $\mathcal{W}_{x,\mathbf{k}}$ are nontrivial $p_y^{\nu_x^\pm,1} = p_y^{\nu_x^\pm,2} = 1/2$. On the other hand, for $\mathcal{W}_{y,\mathbf{k}}$ only $p_x^{\nu_y^\pm,1}$ is nonzero, such that Eq. (10) gives $q_{xy} = 1/2$, signaling a nontrivial TQI. In the Supplemental Material we further confirm these values of the topological invariants by showing the phase transitions that occur between Wannier bands as a function of model parameters $\beta_{1,2}$, V_z, and μ. Note that since $|p_x^{\text{edge}}| = |p_y^{\text{edge}}| = |Q_{\text{corner}}| = 1/2$, as shown in Fig. 2, the index $q_{xy} = 1/2$ defined in Eq. (10) represents the physical quadrupole moment of this system.

Conclusion. We have shown that anomalous topological phases, previously considered unique to periodically driven systems, can occur in time-independent HOTIs. We have introduced an example of such an anomalous HOTI, in which the unitary Wilson loop has topological properties analogous to those of an anomalous Floquet operator. Topological boundary states appear both at 0 and at π values of the eigenphase, leading to a system with quantized edge polarizations and corner charges, but in which the nested Wilson loop index [Eqs. (7) and (8)] vanishes. A bulk invariant has been introduced [Eq. (10)], which takes into account the topological properties of each individual Wannier band, as opposed to those of the entire Wannier sector.

There are, however, important differences between the topology of a Wilson loop and that of the Floquet operator describing a driven system. In Floquet systems, observing topological phases is often hindered by the requirement of filling specific bands [59]. Further, when interactions are present, Floquet band populations are known to evolve towards a featureless infinite temperature state [60,61], unless the system is many-body localized. In contrast, in static HOTIs there is no notion of "filling" for the bands of the Wilson loop. The latter simply describe the positions of ground-state quasiparticles relative to the unit cells, and can be defined also in interacting systems [62,63]. As such, HOTIs may provide a way to observe anomalous phases, while mitigating the above-mentioned difficulties.

Our work bridges the gap between the study of topological phases in static and time-periodic systems, and as such opens many different directions of future research. For instance, anomalous HOTIs can be extended to higher multipole moments, and we conjecture that a three-dimensional (3D) array of coupled nanowires would realize a system with corner charges and an anomalous octupole index. Further, it is interesting to consider whether both 0 and π modes can occur in a system with only two Wannier bands, such as the one of Fig. 1. In that case, neither the index of Eq. (8) nor that of Eq. (10) would be adequate to characterize the nontrivial nature of the phase, prompting the search for other topological invariants. Finally, we remark that anomalous phases are not restricted to insulating systems, and they should be possible also in higher-order topological semimetals. In fact, the gapless Wannier spectrum shown in Fig. 4(d) of Ref. [64] shows protected Dirac cones occurring simultaneously at $\nu = 0$ and

$\nu = \pm 1/2$, a behavior usually associated with anomalous Floquet semimetals [65–68].

Acknowledgments. We thank Ulrike Nitzsche for technical assistance.

[1] D. J. Thouless, M. Kohmoto, M. P. Nightingale, and M. den Nijs, Quantized Hall Conductance in a Two-Dimensional Periodic Potential, Phys. Rev. Lett. **49**, 405 (1982).

[2] C. L. Kane and E. J. Mele, $\mathbb{Z}_2$ Topological Order and the Quantum Spin Hall Effect, Phys. Rev. Lett. **95**, 146802 (2005).

[3] M. Z. Hasan and C. L. Kane, Colloquium: Topological insulators, Rev. Mod. Phys. **82**, 3045 (2010).

[4] X.-L. Qi and S.-C. Zhang, Topological insulators and superconductors, Rev. Mod. Phys. **83**, 1057 (2011).

[5] B. A. Bernevig, *Topological Insulators and Topological Superconductors* (Princeton University Press, Princeton, NJ, 2013).

[6] W. A. Benalcazar, B. A. Bernevig, and T. L. Hughes, Quantized electric multipole insulators, Science **357**, 61 (2017).

[7] W. A. Benalcazar, B. A. Bernevig, and T. L. Hughes, Electric multipole moments, topological multipole moment pumping, and chiral hinge states in crystalline insulators, Phys. Rev. B **96**, 245115 (2017).

[8] J. Langbehn, Y. Peng, L. Trifunovic, F. von Oppen, and P. W. Brouwer, Reflection-Symmetric Second-Order Topological Insulators and Superconductors, Phys. Rev. Lett. **119**, 246401 (2017).

[9] S. Hayashi, Topological invariants and corner states for Hamiltonians on a three-dimensional lattice, Commun. Math. Phys. **364**, 343 (2018).

[10] Z. Song, Z. Fang, and C. Fang, $(d-2)$-Dimensional Edge States of Rotation Symmetry Protected Topological States, Phys. Rev. Lett. **119**, 246402 (2017).

[11] F. Schindler, A. M. Cook, M. G. Vergniory, Z. Wang, S. S. P. Parkin, B. A. Bernevig, and T. Neupert, Higher-order topological insulators, Sci. Adv. **4**, 0346 (2018).

[12] F. Schindler, Z. Wang, M. G. Vergniory, A. M. Cook, A. Murani, S. Sengupta, A. Yu. Kasumov, R. Deblock, S. Jeon, I. Drozdov, H. Bouchiat, S. Guéron, A. Yazdani, B. A. Bernevig, and T. Neupert, Higher-order topology in bismuth, Nat. Phys. **14**, 918 (2018).

[13] Y. Wang, M. Lin, and T. L. Hughes, Weak-pairing higher order topological superconductors, Phys. Rev. B **98**, 165144 (2018).

[14] M. Ezawa, Higher-Order Topological Insulators and Semimetals on the Breathing Kagome and Pyrochlore Lattices, Phys. Rev. Lett. **120**, 026801 (2018).

[15] M. Ezawa, Magnetic second-order topological insulators and semimetals, Phys. Rev. B **97**, 155305 (2018).

[16] M. Ezawa, Strong and weak second-order topological insulators with hexagonal symmetry and $\mathbb{Z}_3$ index, Phys. Rev. B **97**, 241402(R) (2018).

[17] E. Khalaf, Higher-order topological insulators and superconductors protected by inversion symmetry, Phys. Rev. B **97**, 205136 (2018).

[18] V. Dwivedi, C. Hickey, T. Eschmann, and S. Trebst, Majorana corner modes in a second-order Kitaev spin liquid, Phys. Rev. B **98**, 054432 (2018).

[19] G. van Miert and C. Ortix, Higher-order topological insulators protected by inversion and rotoinversion symmetries, Phys. Rev. B **98**, 081110 (2018).

[20] M. Ezawa, Minimal models for Wannier-type higher-order topological insulators and phosphorene, Phys. Rev. B **98**, 045125 (2018).

[21] C.-H. Hsu, P. Stano, J. Klinovaja, and D. Loss, Majorana Kramers Pairs in Higher-Order Topological Insulators, Phys. Rev. Lett. **121**, 196801 (2018).

[22] Z. Yan, F. Song, and Z. Wang, Majorana Corner Modes in a High-Temperature Platform, Phys. Rev. Lett. **121**, 096803 (2018).

[23] Q. Wang, C.-C. Liu, Y.-M. Lu, and F. Zhang, High-Temperature Majorana Corner States, Phys. Rev. Lett. **121**, 186801 (2018).

[24] L. Trifunovic and P. Brouwer, Higher-order bulk-boundary correspondence for topological crystalline phases, arXiv:1805.02598.

[25] M. Geier, L. Trifunovic, M. Hoskam, and P. W. Brouwer, Second-order topological insulators and superconductors with an order-two crystalline symmetry, Phys. Rev. B **97**, 205135 (2018).

[26] T. Liu, J. J. He, and F. Nori, Majorana corner states in a two-dimensional magnetic topological insulator on a high-temperature superconductor, arXiv:1806.07002.

[27] M. Serra-Garcia, R. Süsstrunk, and S. D. Huber, Observation of quadrupole transitions and edge mode topology in an LC network, arXiv:1806.07367.

[28] M. Serra-Garcia, V. Peri, R. Süsstrunk, O. R. Bilal, T. Larsen, L. G. Villanueva, and S. D. Huber, Observation of a phononic quadrupole topological insulator, Nature (London) **555**, 342 (2018).

[29] C. W. Peterson, W. A. Benalcazar, T. L. Hughes, and G. Bahl, A quantized microwave quadrupole insulator with topologically protected corner states, Nature (London) **555**, 346 (2018).

[30] X. Zhang, H.-X. Wang, Z.-K. Lin, Y. Tian, B. Xie, M.-H. Lu, Y.-F. Chen, and J.-H. Jiang, Observation of second-order topological insulators in sonic crystals, arXiv:1806.10028.

[31] S. Imhof, C. Berger, F. Bayer, J. Brehm, L. W. Molenkamp, T. Kiessling, F. Schindler, C. H. Lee, M. Greiter, T. Neupert, and R. Thomale, Topolectrical-circuit realization of topological corner modes, Nat. Phys. **14**, 925 (2018).

[32] P. Sessi, D. D. Sante, A. Szczerbakow, F. Glott, S. Wilfert, H. Schmidt, T. Bathon, P. Dziawa, M. Greiter, T. Neupert, G. Sangiovanni, T. Story, R. Thomale, and M. Bode, Robust spin-polarized midgap states at step edges of topological crystalline insulators, Science **354**, 1269 (2016).

[33] T. Kitagawa, E. Berg, M. Rudner, and E. Demler, Topological characterization of periodically driven quantum systems, Phys. Rev. B **82**, 235114 (2010).

[34] N. H. Lindner, G. Refael, and V. Galitski, Floquet topological insulator in semiconductor quantum wells, Nat. Phys. **7**, 490 (2011).

[35] T. Kitagawa, M. A. Broome, A. Fedrizzi, M. S. Rudner, E. Berg, I. Kassal, A. Aspuru-Guzik, E. Demler, and A. G. White, Observation of topologically protected bound states in photonic quantum walks, Nat. Commun. **3**, 882 (2012).

[36] F. Nathan and M. S. Rudner, Topological singularities and the general classification of Floquet–Bloch systems, New J. Phys. **17**, 125014 (2015).

[37] A. C. Potter, T. Morimoto, and A. Vishwanath, Classification of Interacting Topological Floquet Phases in One Dimension, Phys. Rev. X **6**, 041001 (2016).

[38] D. V. Else and C. Nayak, Classification of topological phases in periodically driven interacting systems, Phys. Rev. B **93**, 201103 (2016).

[39] M. S. Rudner, N. H. Lindner, E. Berg, and M. Levin, Anomalous Edge States and the Bulk-Edge Correspondence for Periodically Driven Two-Dimensional Systems, Phys. Rev. X **3**, 031005 (2013).

[40] P. Titum, E. Berg, M. S. Rudner, G. Refael, and N. H. Lindner, Anomalous Floquet-Anderson Insulator as a Nonadiabatic Quantized Charge Pump, Phys. Rev. X **6**, 021013 (2016).

[41] F. Nathan, D. Abanin, E. Berg, N. H. Lindner, and M. S. Rudner, Stability of anomalous Floquet insulators, arXiv:1712.02789.

[42] A. Kundu, M. Rudner, E. Berg, and N. H. Lindner, Quantized large-bias current in the anomalous Floquet-Anderson insulator, arXiv:1708.05023 .

[43] L. J. Maczewsky, J. M. Zeuner, S. Nolte, and A. Szameit, Observation of photonic anomalous Floquet topological insulators, Nat. Commun. **8**, 13756 (2017).

[44] S. Mukherjee, A. Spracklen, M. Valiente, E. Andersson, P. Öhberg, N. Goldman, and R. R. Thomson, Experimental observation of anomalous topological edge modes in a slowly driven photonic lattice, Nat. Commun. **8**, 13918 (2017).

[45] W. P. Su, J. R. Schrieffer, and A. J. Heeger, Solitons in Polyacetylene, Phys. Rev. Lett. **42**, 1698 (1979).

[46] F. Wilczek and A. Zee, Appearance of Gauge Structure in Simple Dynamical Systems, Phys. Rev. Lett. **52**, 2111 (1984).

[47] M. V. Berry, Quantal phase factors accompanying adiabatic changes, Proc. R. Soc. London, Ser. A **392**, 45 (1984).

[48] See Supplemental Material at http://link.aps.org/supplemental/10.1103/PhysRevB.98.201114, which contains Refs. [6,7,46,47,49,50,69,70], for a detailed description of the procedure used to compute the Wilson loops, the polarizations, and the code used for our simulations. In addition, we provide more details on the two models and show topological phase transitions of the Wannier bands.

[49] Y. Oreg, G. Refael, and F. von Oppen, Helical Liquids and Majorana Bound States in Quantum Wires, Phys. Rev. Lett. **105**, 177002 (2010).

[50] R. M. Lutchyn, J. D. Sau, and S. Das Sarma, Majorana Fermions and a Topological Phase Transition in Semiconductor-Superconductor Heterostructures, Phys. Rev. Lett. **105**, 077001 (2010).

[51] A. Yu. Kitaev, Unpaired Majorana fermions in quantum wires, Phys. Usp. **44**, 131 (2001).

[52] J. C. Y. Teo and C. L. Kane, Topological defects and gapless modes in insulators and superconductors, Phys. Rev. B **82**, 115120 (2010).

[53] J. C. Budich and E. Ardonne, Equivalent topological invariants for one-dimensional Majorana wires in symmetry class *D*, Phys. Rev. B **88**, 075419 (2013).

[54] L. Jiang, T. Kitagawa, J. Alicea, A. R. Akhmerov, D. Pekker, G. Refael, J. I. Cirac, E. Demler, M. D. Lukin, and P. Zoller, Majorana Fermions in Equilibrium and in Driven Cold-Atom Quantum Wires, Phys. Rev. Lett. **106**, 220402 (2011).

[55] A. Kundu and B. Seradjeh, Transport Signatures of Floquet Majorana Fermions in Driven Topological Superconductors, Phys. Rev. Lett. **111**, 136402 (2013).

[56] Q.-J. Tong, J.-H. An, J. Gong, H.-G. Luo, and C. H. Oh, Generating many Majorana modes via periodic driving: A superconductor model, Phys. Rev. B **87**, 201109(R) (2013).

[57] S. Yao, Z. Yan, and Z. Wang, Topological invariants of Floquet systems: General formulation, special properties, and Floquet topological defects, Phys. Rev. B **96**, 195303 (2017).

[58] X. Yang, B. Huang, and Z. Wang, Floquet topological superfluid and Majorana zero modes in two-dimensional periodically driven Fermi systems, Sci. Rep. **8**, 2243 (2018).

[59] L. D'Alessio and M. Rigol, Dynamical preparation of Floquet Chern insulators, Nat. Commun. **6**, 8336 (2015).

[60] L. D'Alessio and M. Rigol, Long-time Behavior of Isolated Periodically Driven Interacting Lattice Systems, Phys. Rev. X **4**, 041048 (2014).

[61] A. Lazarides, A. Das, and R. Moessner, Equilibrium states of generic quantum systems subject to periodic driving, Phys. Rev. E **90**, 012110 (2014).

[62] G. Ortiz and R. M. Martin, Macroscopic polarization as a geometric quantum phase: Many-body formulation, Phys. Rev. B **49**, 14202 (1994).

[63] S.-S. Lee and S. Ryu, Many-Body Generalization of $\mathbb{Z}_2$ Topological Invariant for the Quantum Spin Hall Effect, Phys. Rev. Lett. **100**, 186807 (2008).

[64] M. Lin and T. L. Hughes, Topological quadrupolar semimetals, arXiv:1708.08457.

[65] L. Zhou, C. Chen, and J. Gong, Floquet semimetal with Floquet-band holonomy, Phys. Rev. B **94**, 075443 (2016).

[66] R. W. Bomantara, G. N. Raghava, L. Zhou, and J. Gong, Floquet topological semimetal phases of an extended kicked Harper model, Phys. Rev. E **93**, 022209 (2016).

[67] H. Wang, L. Zhou, and Y. D. Chong, Floquet Weyl phases in a three-dimensional network model, Phys. Rev. B **93**, 144114 (2016).

[68] S. Higashikawa, M. Nakagawa, and M. Ueda, Floquet chiral magnetic effect, arXiv:1806.06868.

[69] R. Resta, Quantum-Mechanical Position Operator in Extended Systems, Phys. Rev. Lett. **80**, 1800 (1998).

[70] L. Fidkowski, T. S. Jackson, and I. Klich, Model Characterization of Gapless Edge Modes of Topological Insulators Using Intermediate Brillouin-Zone Functions, Phys. Rev. Lett. **107**, 036601 (2011).